Interfacial Water Manipulation with Ionic Liquids for the Oxygen Reduction Reaction

Yawei Li[1,2], Arnav Malkani[3], Ramchandra Gawas[2], Saad Intikhab[2], Bingjun Xu[3,4], Maureen Tang[2], Joshua Snyder[2*]

[1] *School of Chemistry and Chemical Engineering, Shanxi University, Taiyuan 030006, China*

[2] *Department of Chemical and Biological Engineering, Drexel University, Philadelphia, PA 19104, USA*

[3] *College of Chemistry and Molecular Engineering, Peking University, Beijing 100871, China*

[4] *Department of Chemical and Biomolecular Engineering, University of Delaware, Newark, DE 19716, USA*

**Corresponding author: jds43@drexel.edu*

Abstract

The role that interfacial water plays in both promoting and inhibiting the electrochemical oxygen reduction reaction (ORR) remains somewhat mysterious and controversial. Here we use electroanalytical chemistry, spectroscopy, and microkinetic modeling to probe the impact of hydrophobic ionic liquid (IL) thin films on interfacial water structure and its role in promoting or inhibiting the ORR. Through the use of *in situ* ATR-SEIRAS, we find that the IL thin films limit the content of water at the interface and prevent the formation of hydrogen bond stabilized water organization. The impact of this exclusion of water on the promotion of the ORR is through the reduced coverage of OH_{ad} spectator species. The decreased solvation of "active" OH_{ad} species weakens its interaction with the catalyst surface, lowering the barrier to the last step in the ORR mechanism. This "destabilized" OH_{ad} impact on ORR kinetics is confirmed through a microkinetic model. The results presented here highlight the mechanistic pathway through which hydrophobic ILs enhance ORR kinetics and point to pathways to both further improve this performance

enhancement and the potential for integration of hydrophobic ILs into other technologically relevant elementary electrochemical reactions.

Keywords

Oxygen reduction reaction, ionic liquids, single crystal electrodes, fuel cells, electrocatalysis

1. Introduction

Electrochemical energy conversion and storage technologies are critical for any level of transition to a more renewable sourced energy economy. Commercial relevance, however, requires an improvement in electrocatalytic activity and selectivity for the governing electrochemical reactions as well as improved material durability with a concomitant reduction in cost.[1–3] The efficiency of electrochemical energy conversion and storage devices is defined by the rate and selectivity of electrochemical processes occurring at and within electrodes, catalytic or otherwise. For electrocatalytically driven processes, research emphasis to this point has been mostly materials focused, where the path forward has been guided by reactive species binding activity descriptors.[1,4,5] For broadly studied electrochemical reactions, particularly those with multiple intermediate species such as the oxygen reduction reaction (ORR), a solid catalyst centered approach, looking at different alloy compositions and nanostructures, has at this point lead to a plateau in both catalyst and device performance.[1] An additional limitation for a solid catalyst centered focus, particularly for multi-intermediate reactions, is the imposition of a thermodynamically defined minimum overpotential. This minimum overpotential is established by the adsorption free energy scaling behavior among the reactive intermediates[6–10] and is difficult to overcome through the traditional knobs that are turned for catalyst development including structure, compositional profile, and nanoscale morphology.[11–15]. While several solid catalyst-

based strategies have been proposed to break this scaling behavior,[1] we have yet to see real practical implementation and success of these proposed strategies.

In order to achieve further progress, one strategy is to shift focus away from the catalyst and toward the interface.[16] The unique properties of ionic liquids (IL) including ionic conductivity, negligible vapor pressure, wide electrochemical potential stability window, and high oxygen solubility in addition to the large library of organic chemical species readily available to aid in the synthetic tuning of these and other physical properties make ILs ideally suited for chemical tailoring of the electrocatalytic interface.[17] Multiple groups have demonstrated the capability of IL modifications to enhance the ORR activity with a range of different IL chemistries.[18–29] There remain, however, many fundamental questions as to the true nature of the cooperative interaction between IL, catalyst, reactant, and electrolyte.[22,23,25]

Although it is well known that electrochemical reaction kinetics are strongly coverage dependent,[30–33] the role of water in influencing electrochemical kinetics for reactions involving multiple adsorbed intermediates is often overlooked. The unparalleled ORR activity on $Pt_3Ni(111)$ is a direct consequence of the reduced adsorption free energy of oxygenated species and the reduction in coverage of spectator species such as OH_{ad}.[4] In addition to electronic properties of the surface, spectator coverage is related to both the defect density on the surface, where OH_{ad} nucleates at low coordinated sites, and OH_{ad} intermediate stabilization through hydrogen bonding with near-surface solvent water (see **Figure 1a**).[34–36] The ORR activity of the three low-index facets of Pt in a “non-adsorbing” electrolyte shows a strong structural sensitivity[37,38]. As the ORR mechanism, whether dissociative or associative, involves breaking of an O—O bond as a possible rate determining step, it is easy to think of the close-packed surface of the (111) face as being the most active of the low index facets. The presence of “free" neighboring Pt atoms will favor

bidentate adsorption which could promote O—O bond breaking. Evidence of the role of these "free" neighboring sites can be seen in the trend in ORR current density at high overpotentials on Pt (111).[4,39,40] As the ORR overpotential approaches potentials where underpotentially deposited hydrogen (HUPD) can be formed, the current density is found to decrease on Pt(111). The increasing coverage of adsorbed H with increasing overpotential limits the total number of "free" neighboring Pt sites, forcing O_2 to adsorb through only one oxygen atom, and increasing the probability of hydrogen peroxide desorbing as a product. The reduction in ORR current density in this region is then a partial shift away from 4-electron ORR and toward 2-electron ORR.[39,40] The cubic (100) face could also favor bidentate adsorption, but the adsorption free energy of oxygenated intermediates is too strong for the (100) face, making it the least active low index facet for ORR at low pH.[41] The ORR activity is significantly higher on Pt(111), however, it is found to be highest on Pt(110).[4,37] This is somewhat counterintuitive as the atomically "rough" surface of both reconstructions of Pt(110) 1×2 and 1×1 (see **Figure 1b**) would be expected to have the highest coverage of spectator oxygenated species.[42] Indeed, the presence of OH_{ad} at potentials as low as 0.3 V vs. RHE and the early onset of the electrooxidation of CO in comparison to the Pt(111) face is evidence of the higher steady-state coverage of OH_{ad}.[43] Comparatively, the steady-state coverage of spectator OH_{ad} on Pt(111), within an ORR relevant potential window, is lower as the defect density, limited to the minimal number of step edges on the crystal surface, is significantly lower.[44] It is not intuitively satisfying then that Pt(110) is more active than Pt(111). However, in addition to spectator OH_{ad}, we also have to consider site occupying/blocking reactive oxygenated species such as OH_{ad}/OOH_{ad}/O_{ad} that are direct participators in the electrochemical reaction. Considering both the associative and dissociative mechanisms, OH_{ad} must be removed as one of the final reaction steps. One distinctive difference between the (110) and (111) facets of Pt is the interaction

of those surfaces with water. For Pt(111), it has been demonstrated that an ordered "ice-like" water network can be formed on the surface, **Figure 1(a)**. The atomically flat, close-packed surface of Pt(111) with comparatively minimal oxygenated species coverage[36,45], promotes the formation of a hexagonal hydrogen bonded water network with $(\sqrt{3} \times \sqrt{3})R30^\circ$ symmetry.[46–50] The catalytic impact of this ordered, hydrogen bonded water network at the Pt(111) surface can be manifested is a few ways:

(1) The presence of an ordered, hydrogen bonded water network stabilizes OH_{ad}.[51] This can both increase the coverage of spectator OH_{ad} and reduce the rate of OH_{ad} removal in the final elementary steps in both the associative and dissociative ORR reaction mechanisms.

(2) The rigidity of this hydrogen bonded interfacial water network, which is both a function of the interfacial electric field strength and population of adsorbed oxygenated species, can impede ion and reactant/product transport through the compact double layer.[52,53] Proton-coupled electron transfers (PCET) also require fluid water to facilitate hydrogen bond rearrangement during the electrochemical conversion.

(3) The solvation of OH_{ad} and OOH_{ad} intermediates yields a disparate change to their binding energies, increasing OH_{ad} by 0.5 eV and OOH_{ad} by 0.25 eV,[8] which can exacerbate ORR scaling behavior.[6]

In contrast to Pt(111), the atomic corrugations of Pt(110), see schematic in **Figure 1(b)**, prevent or limit the formation of this ordered water network.[54] It is then potentially this difference in the degree of interaction between the water and the catalyst surface that yields the higher ORR activity for Pt(110).[45]

Significant fundamental efforts focused on electroanalytical characterization of the water/catalyst interface have provided a certain degree of understanding of the impact of this interface on electrocatalytic reaction rates and selectivity[46,48,62,50,55–61]. Direct implementation of strategies utilizing this insight, in contrast to solid catalyst focused strategies, are limited. One of the notable exceptions to this, particularly for ORR electrocatalysis, is the use of hydrophobic ionic liquids (IL).[18–29] There is clear evidence that the presence of these hydrophobic ILs, both protic and aprotic, reduce the coverage of OH_{ad} at ORR relevant potentials by shifting the onset potential for OH_{ad}/O_{ad} formation positive[22,25,27]. While this is a potential source of the observed ORR activity improvement in the presence of the IL, specifically the limiting of spectator coverage and increase in free site density, there have been other proposed sources of ORR activity enhancement. These include: (1) increased interfacial O_2 concentration due to the higher O_2 solubility in ILs,[19] (2) minimization of adsorbed intermediate adsorption free energy scaling behavior due to reduction in adsorbed species solvation[8]; (3) faster/lower barrier proton transfers from the protic sites of the IL to adsorbed intermediates[21]. There has been no direct correlation between O_2 solubility and ORR activity found[25]. Correlations for proton transfers fit well with protic ILs, however, these cannot explain why similar activity enhancements can be achieved with aprotic ILs[23].

In this paper, through a systematic study of well-defined single crystal electrodes, *in situ* attenuated total reflection surface enhanced infrared absorption spectroscopy (ATR-SEIRAS), and microkinetic modeling we demonstrate that ILs act to prevent the formation of an ordered ice-like water structure, limiting the degree of solvation of both spectator and reactive OH_{ad}. The resultant increase in free-site coverage and reduced barrier for OH_{ad} conversion to water yields an enhanced ORR activity. Therefore, it is the exclusion of interfacial water, while maintaining an interfacial

environment that still facilitates water, ion, and reactant transport, that is the source of the ORR activity enhancement for IL incorporated electrocatalysts.

2. Experimental

Electrode preparation. Pt(111) and Pt(110) (Princeton Scientific, 5 mm dia. discs) single crystals were inductively annealed at 1100 ºC for 10 min under Ar/3% H_2 (Airgas) flow. The annealed discs were cooled slowly to room temperature under Ar/3% H_2 flow and then protected with a droplet of ultrapure water (18.2 MΩ.cm, TOC < 3 ppb, Millipore) for transferring to the rotating disk electrode (RDE) half-cell. All single crystals are immersed in the electrolyte under potential control, 0.1 V vs. reversible hydrogen electrode (RHE).

IL deposition. The electrodes for electrochemical measurements were coated with ILs through a sequential capacitive deposition (SCD) method as outlined previously.[22] Briefly, single crystal discs supported in an RDE collet were immersed in a 0.1 M Li[beti] aqueous electrolyte (beti: bis(perfluoroethylsulfonyl)imide, iolitec, 99%) with a constant applied potential of 0.55 V vs. RHE and a rotation of 300 rpm for 15 min. The electrode was then transferred into DI water while rotating at 300 rpm for 30 seconds to wash away residual ions. Next, the $[beti]^-$ adsorbed electrode was rested in a 0.05 M aqueous [MTBD] (7-methyl-1,5,7-triazabicyclo[4.4.0]dec-5-ene, Sigma Aldrich, 98%) solution, at 300 rpm for 10 min. Finally, the electrode was transferred back into DI water to wash away impurities while rotating at 300 rpm for 10 min.

The electrodes for *in situ* ATR-SEIRAS were coated with IL thin films through spin coating. The [MTBD][beti] (**Figure S1**) IL was prepared according to a previously reported procedure.[63] IL solutions were prepared by diluting the as-made IL by a factor of 10 with ultrapure 2-propanol (99.8%, Sigma-Aldrich) and sonicating for 30 min. The solution drop volume for

coating of the electrodes was tailored to ensure a 10 µm IL film thickness following evaporation of the solvent under electrode rotation and Ar flow. Rotation rate was slow enough to prevent loss of solution, ensuring reproducible film thicknesses controlled by the solution concentration and drop volume.

Electrochemical measurements. All electrochemical measurements were performed at room temperature with an RDE from Pine Instruments controlled by a Metrohm Autolab potentiostat (PGSTAT302N). The hanging meniscus RDE configuration[37] was used for most measurements. The counter electrode was Pt mesh (99.9%, Alfa Aesar) bonded to the end of a Pt wire (99.9%, Alfa Aesar), and a Ag/AgCl (BASi) electrode was used as a reference. The electrolytes were freshly prepared using ultrapure water (18.2 MΩ.cm, TOC < 3 ppb, Millipore). Cyclic voltammetry (CV) profiles were obtained in Ar (99.999%, Airgas) purged electrolyte with a potential range of 0.05 – 1.2 V vs. RHE at a scan rate of 50 mV s^{-1}. ORR polarization curves were obtained through potential cycling between 0.02 – 1.0 V vs. RHE in O_2 (99.999%, Airgas) saturated electrolyte at a scan rate of 20 mV s^{-1} and a rotation rate of 1600 rpm. All polarization curves in this paper are normalized by the geometric surface area of the single crystal electrodes (0.196 cm^2). All electrochemical measurements were repeated at least three times to ensure reproducibility. Kinetic current densities for ORR were calculated using the Koutecky-Levich equation to adjust for mass transport limitations:

$$\frac{1}{i_n} = \frac{1}{i_k} + \frac{1}{i_d} \qquad \text{(Eq. 1)}$$

where, i_n is the measured current density at 0.9 V vs. RHE, i_d is the diffusion-limited current density at 0.4 V vs. RHE, and i_k is the kinetic current density at 0.9 V vs. RHE.

***in situ* ATR-SEIRAS.** A two-compartment, three-electrode glass cell was used for all spectroscopic measurements. A schematic of the setup used for spectroscopic studies can be found in previous publications.[64,65] One compartment contains a graphite counter electrode and is separated from the other by a Nafion ion exchange membrane (IEM, Nafion 211, Fuel Cell Store). The other compartment contains the Au coated working electrode, a Ag/AgCl reference electrode (3.0 M NaCl, BASi), and gas inlet and purge lines. The electrodes were connected to a potentiostat (Solartron 1260/1287) that was used for electrochemical measurements. The cell was integrated into the Agilent Technologies Cary 660 FTIR spectrometer equipped with a liquid nitrogen-cooled MCT detector. All spectra were collected at a 4 cm^{-1} spectral resolution and are presented in absorbance difference units where a positive and negative peak signifies an increase and decrease in the interfacial species, respectively.

3. Results and Discussion

The direct impact of [MTBD][beti] IL thin films, formed through sequential capacitive deposition (SCD)[22], on the voltammetry and ORR activity of Pt(111) and Pt(110) single crystals is shown in **Figure 2**. There is minimal change to the charge associated with the underpotential deposition of hydrogen (H_{UPD}) indicating minimal surface Pt site blocking by the IL thin film, **Figures 2(a)** and **(b)**. Additionally, a clear shift in the onset/peak potential as well as the reduction in total charge associated with OH_{ad}/O_{ad} formation is indicative of the presence of ILs at a Pt interface.[18,22,23,26] In agreement with previous works assessing the impact of ILs,[18,19,22–24] even [MTBD][beti] specifically, on the ORR activity of Pt nanomaterials, we show in **Figure 2(c)** and **(d)** the expected enhancement in ORR activity for Pt(111) and Pt(110). What is new here is that we find the degree of ORR activity enhancement is crystallographic orientation dependent. As shown in **Figure 3** and quantified in **Table S1**, the addition of the SCD [MTBD][beti] thin film to

the Pt(111) surface yields a 2X improvement in the kinetic current density at 0.9 V vs. RHE while that on Pt(110) yields a 1.5X improvement. At its face, this result is somewhat counterintuitive. The atomically corrugated surface of Pt(110) will have a higher nominal coverage of OH_{ad}/O_{ad} in comparison to Pt(111).[37] It would then be expected that if the dominant impact of the hydrophobic IL is to reduce the coverage of spectator OH_{ad} or minimize the adsorption free energy of reactive OH_{ad}, the larger effect would be seen for Pt(110) as there is more nominal OH_{ad}/O_{ad} coverage at higher ORR overpotentials.[37] A case can be made for the similarities between the structural sensitivity of the ORR kinetic activity with and without IL. We propose that there are potentially two things at play here: (1) the atomic corrugation of the Pt(110) surface prevents the formation of an ordered, hydrogen bonded water network, lowering the probability for the presence of stabilized H_2O-OH_{ad} complexes, and (2) the ORR active sites on a Pt(110) surface consist of the trough of atoms beneath the lower coordinated rows, see **Figure 1(b)**, and the decoration of those lower coordinated atoms lining the trough with oxygenated species, sterically protects the active sites within the trough, preventing passivation and limiting any interaction between water and the adsorbed intermediates at the active sites. The limitation of the interaction between water and the active sites as well as the steric protection of the active trough sites on Pt(110) can potentially explain the improved ORR kinetics at pH 1 for a bare Pt(110) over a bare Pt(111). If we think about this now in the context of the ORR activity trend observed for the IL covered surfaces, we can propose a potential hypothesis: the presence of the hydrophobic ILs reduces the concentration of water at the metal/electrolyte interface, lowering the degree of solvation of adsorbed species and preventing the formation of an ordered, hydrogen-bonded water network. From the CVs in **Figure 2(a)** and **(b)**, we know that the total coverage of OH_{ad}/O_{ad} is reduced for both Pt(111) and Pt(110). However, as we have mentioned previously, it is not just a change in spectator species

coverage that is relevant, the impact of the solvation of reactive oxygenated intermediates on their adsorption free energy and reactivity could have a large impact as well. For Pt(111), the presence of the IL both lowers the coverage of site blocking OH_{ad}/O_{ad}, as evidenced by the CVs in **Figure 2(a)**, and potentially reduces the degree of solvation of reactive intermediates. The wide, flat, close-packed terraces favor the formation of ordered water structures which will tend to maximize adsorbed species solvation.[51] Therefore, the impact of removing that water structure through the addition of the hydrophobic IL to the interface is expected to be significant, see **Figure 3**. If we contrast this with the Pt(110) surface, while a reduction in OH_{ad}/O_{ad} coverage is observed, the steric protection of the trough active sites even in the absence of the hydrophobic IL, limits the degree of reactive intermediate solvation. Therefore, the impact of the IL on ORR reactivity is diminished in comparison as the atomic scale structure of the Pt(110) surface already limits the degree of water interaction and prevents the formation of an ordered water network.

We can support our hypothesis by probing the state and content of water at a metal/electrolyte interface with attenuated total reflectance surface enhanced infrared absorption spectroscopy (ATR-SEIRAS). ATR-SEIRAS has many advantages over traditional IR spectroscopy, namely the ability to interface with bulk electrolyte and have a high degree of surface sensitivity, sampling only 5-10 nm beyond the metal/electrolyte interface[65]. Previous work has attributed specific wave numbers in the SEIRA spectra to highly hydrogen bonded ice-like water (3290 cm^{-1}) and more weakly associating non-hydrogen bonded water (1600, 1620 cm^{-1})[65–67]. The spectra in **Figure 4(a)** and **(b)**, in the presence of an IL thin film, show a distinct absence, or significant reduction, of all features associated with interfacial water in comparison to a bare metal surface.[65–67] Au electrodes, rather than Pt, were used as there exists disagreement as to the assigning of some water peaks on Pt[68–71] and some concern as to the relative reliability of the

difference spectra[72]. This result is expected as the hydrophobic ILs unsurprisingly limits the content of water at the metal surface. However, it is known that these ILs have a nominal water solubility that can range up to several hundred ppm.[73] We argue that this nominal water solubility is critical for the operation of the IL at an ORR catalyst interface. While the IL used here is protic, the anhydrous ionic/protonic conductivity is much lower than that required to maintain high ORR turnover rates.[25] Integration of water, likely in a semi-phase segregated morphology creating water/ionic channels, leads to dramatic enhancements in ionic conductivity.[74] Additionally, if the IL has some water solubility, the water formed at the catalyst surface during ORR has a place to go, diffusing out into the bulk electrolyte. **Figure 4(c)** compares two ATR-SEIRAS spectra on a Au electrode in alkaline electrolyte, one spectra with a thin [MTBD][beti] film on the Au electrode and one without. We have chosen to use a Au electrode in alkaline electrolyte as the relevant bands for OH_{ad} are more clear under these conditions.[65] The band clearly moves from ~3400 to 3506 cm^{-1} as the potential is increased. This feature has been attributed to adsorbed hydroxide (OH_{ad})[65]. In the presence of the IL thin film, there is a clear reduction in peak intensity at all potentials, signifying a reduced coverage of OH_{ad}. The peak intensity of this feature increases with increasing potential but begins to decrease at potentials above 0.2 V vs. RHE. This reduction in intensity does not imply a reduction in the coverage of OH_{ad}, which would disagree with intuition and all other measurements of oxygenated species coverage with potential, e.g., CVs.[65] A definitive reason for this decrease in intensity is not available, but it has been suggested that there is a broad feature between ~3100—3500 cm^{-1} that is associated with near surface water. This feature is found to decrease with increasing potential and its convolution with the OH_{ad} peak may result in the observed decrease in peak intensity with increasing potentials beyond 0.2 V vs. RHE.[65] The ATR-SEIRAS spectra in **Figure 4** strongly support our hypothesis of water-driven changes to OH_{ad}

coverage, and consequently free-site density, adsorption free energy and reaction step barriers, as the potential source of the ORR activity improvement in the presence of interfacial IL thin films.

Additional voltametric evidence supporting the role of interfacial IL thin films in adjusting the solvation of adsorbed spectator and reactive OH_{ad} is provided in **Figures 5** and **S2**. The role of hydrated alkali metal cations in the solvation and binding of OH_{ad} to metal catalyst surfaces has been well documented.[75–78] For example, the correlation between ORR activity and alkali metal cation identity in alkaline electrolytes scales directly with the hydration energy of the alkali metal cation.[76] The Li^+ cation has the highest solvation energy.[76] Therefore, the degree of interaction between Li^+ solvating water and adsorbed intermediate OH_{ad} leads to the greatest degree of binding energy increase over the unsolvated intermediates in comparison to other alkali metal cations, i.e. K^+. **Figure 5** shows the ORR polarization curves and kinetic current density in 0.1 M LiOH and 0.1 M KOH with and without the hydrophobic cation tetrahexylammonium (THA^+) added to the electrolyte. The THA^+ cations are found to enhance the ORR activity in both electrolytes. Previous work has suggested that THA^+ and other hydrophobic cations enhance ORR activity by limiting the interaction between water and the catalyst surface, reducing oxygenated spectator species coverage.[51] In this way they behave similarly to interfacial ILs in that they yield ORR activity enhancements through the exclusion of near surface water and more optimal species coverage. We have used THA^+ for the measurements in **Figure 5** instead of [MTBD][beti] as alkaline electrolyte will partially neutralize the protic IL. This can result in inconsistent ORR performance between different electrode preparations. Conducting measurements at pH 13 rather than pH 1 further strengthens the impact of hydrated alkali metal cations.[76] The ORR enhancement with the addition of THA^+ cations is likely due to the exclusion of both water and hydrated Li^+ cations from the interface, resulting in both a reduction in OH_{ad} coverage and a weakening of its adsorption. In

Figure 5, we compare the degree of performance enhancement from the THA^+ cations LiOH and KOH electrolytes. In comparison to Li^+, K^+ has a much lower solvation energy.[75,76] This means that the binding and equilibrium coverage of OH_{ad} in KOH is expected to be lower.[76] The degree of ORR improvement with THA^+ electrolyte additives is clearly greater in LiOH than KOH. As the binding and OH_{ad} coverage in KOH is lower than LiOH, the reduced impact of the THA^+ cations fits with the hypothesis that their impact is through the exclusion of water and hydrated cations, resulting in lower spectator coverage and destabilized OH_{ad} intermediate species.

Figure 6 is an additional qualitative measure of the impact of the IL on OH_{ad} coverage. Zero current mixed potential (ZCMP) is a qualitative measure of the oxophilicity of a catalyst surface.[79–81] With a series of rotations rates, the ZCMP is determined by the intersection of hydrogen peroxide oxidation and reduction (HPORR) curves, **Figure 6**. This intersection is the potential at which the probability to oxidize and reduce H_2O_2 are equal. As OH_{ad} is both a reactant (H_2O_2 oxidation) and adsorbed intermediate (H_2O_2 reduction),[79] the value of the ZCMP in the anodic HPORR scan has been suggested to be a measure of the average affinity of the catalyst surface for oxygenated species, i.e. oxophilicity. The more positive the ZCMP, the less oxophilic the surface.[79] In **Figure 6**, we show that the ZCMP shifts positive by approximately 70 mV for a Pt(110) surface that is covered in a [MTBD][beti] IL thin film. Pt(110) is used here rather than Pt(111) as the nominal OH_{ad} coverage is higher due to the lower average coordination of surface Pt atoms. This ensures that the shift in ZCMP between the bare and IL covered surfaces is more visible. However, we include the data for Pt(111) in **Figure S3** where we do in fact see a positive shift in the ZCMP in the presence of the IL thin film. This result further supports the role of interfacial hydrophobic ILs in reducing the surface coverage of oxygenated species by lowering their barrier for removal.

To this point we have presented electroanalytical results that support the hypothesis of the weakened interaction between OH_{ad} and the Pt surface due to reduction in the surface coverage of water in the presence of interfacial IL thin films. However, we do not have a direct quantitative measure of the impact of these hydrophobic species on OH_{ad} adsorption free energy and the subsequent ORR kinetic improvement. We have previously developed an ORR microkinetic model that allows us to fit the voltammetry and polarization curves for Pt(111) modified with hydrophobic ILs.[82] Novelty of this model lies in the incorporation of a coverage dependent adsorption free energy for oxygenated species with a modified Frumkin isotherm. Using our model, we first evaluate the impact of IL modification on OH_{ad} and O_{ad} binding energies by comparing experimental and simulated CVs. **Figure 7(a)** shows a strong qualitative match with the impact of IL thin films on the Pt(111) CV, **Figure 2(a)**. This model CV is obtained by destabilizing or weakening the binding of both OH_{ad} and O_{ad} by 0.025 eV. Simulated polarization curves, using the modified binding energies, **Figure 7(b)**, show a strong fit to the experimental polarization curves in **Figure 2(c)**, supporting the role of IL/water interactions in promoting activity through a destabilization of OH_{ad}, reducing spectator coverage and increasing the number of free-sites. From the model we can also output simulated coverages, **Figure 7(c)**. We see a distinct decrease in OH_{ad} coverage at ORR relevant potentials in the simulated IL case as a result of new equilibrium coverage profiles due to destabilized OH_{ad} and O_{ad}. Interestingly, the opposite is true for O_{ad} coverage, where the 0.025 eV OH_{ad}/O_{ad} destabilization leads to an increase in O_{ad} coverage at mixed kinetic/diffusion ORR potentials, **Figure 7(c)**. We can hypothesize as to the source of this unexpected result: When we weaken OH_{ad} and O_{ad} in our microkinetic model it changes the equilibrium coverage profile, and in this new coverage profile, we see a lower OH_{ad} coverage but higher O_{ad} and free site coverages. A possible explanation could be that as we weaken OH_{ad}, it

makes the final elementary step easier, i.e. the removal of OH_{ad} as water, but makes the previous elementary step, the O_{ad} -> OH_{ad} transition, more difficult. As a result, we get less OH_{ad} and more O_{ad} on the IL covered surface in comparison to the bare surface. In **Figure 7(d)**, we see a strong correlation between increase in potential dependent free-site coverage and improved kinetic current density for Pt(111) modified with IL thin films in comparison with bare Pt(111). In our previous work[82], we have shown that hydrophobic IL thin films change the scaling behavior but the impact of scaling behavior of OH_{ad}/OOH_{ad}/O_{ad} on ORR kinetics is inconsequential for realistic modifications in OH_{ad} adsorption free energy. Additionally, in our previous work[82] we have used our model to explore the role of adsorbed species weakening by separately modifying adsorption free energies of OH_{ad}, O_{ad}, and OOH_{ad}. Our model indicates that ORR kinetic improvements through reduction in interface solvation is dominated by changes in OH_{ad} binding and minimally affected by changes to OOH_{ad} and O_{ad} binding. These microkinetic model results lend further support to the dominant mechanism of ORR enhancement in the presence of hydrophobic IL thin films being the reduction in spectator OH_{ad} coverage, through near surface water exclusion.

Taken together, the data presented here indicate that the dominant mechanism by which interfacial ILs improve ORR activity is through the reduction in coverage of oxygenated spectator species, increasing active site density, and easing the removal of intermediate OH_{ad} during ORR. The key property of ILs contributing to this effect is their hydrophobicity, which can be a function of both anion and cation chemistry. However, maximizing IL hydrophobicity is suboptimal[83] as ORR requires transport of water, protons, and O_2 between the catalyst surface and bulk electrolyte. Further development in IL chemistry may solve the delicate balance between reduced water activity at the surface and sufficient proton concentration and transport to the reactive interface.

4. Conclusion

Ionic liquids as interface modifiers for ORR electrocatalysts have demonstrated utility with a broad range of research groups showing significant enhancements in activity both in the half-cell and PEMFC MEA. The origin of this enhanced activity, while speculated and hypothesized by numerous research groups, remains controversial. The data presented here supports the hypothesis that the dominant mechanism of ORR enhancement at a catalyst/IL interface is through the optimization of the water/catalyst interaction. Through the partial exclusion of water, the hydrophobic IL leads to reduced oxygenated spectator species, i.e. OH_{ad}, coverage which results in increased active site density. Additionally, the reduced solvation of oxygenated intermediates, such as OH_{ad} and O_{ad}, decreases their binding energy, increasing the rate of elementary reaction steps involving these species. Namely, the weakening of OH_{ad} binding through reduced solvation will ease its removal during the final elementary step of the ORR mechanism, improving active site turnover. This conclusion is supported by electroanalytical study of structural sensitivity, in-situ spectroscopy, and microkinetic modeling. Based on these results, a potential path forward is to develop new IL chemistries that further optimize the interaction between the catalyst surface and water while balancing O_2, proton, and water transport between the catalyst and bulk electrolyte.

Supporting Information

Experimental methods, ionic liquid molecular structure, additional supporting experimental data.

Acknowledgements

R.G., M.T., and J.S. acknowledge support from the Department of Energy Office of Energy Efficiency & Renewable Energy through award DE-EE0008434.

References

1. She, Z. W., Kibsgaard, J., Dickens, C. F., Chorkendorff, I., Nørskov, J. K. & Jaramillo, T. F. Combining theory and experiment in electrocatalysis: Insights into materials design. *Science* **355**, 1–12 (2017).

2. Li, Y., Hart, J. L., Taheri, M. L. & Snyder, J. D. Morphological Instability in Topologically Complex, Three-Dimensional Electrocatalytic Nanostructures. *ACS Catal.* **7**, 7995–8005 (2017).

3. Li, Y., Polakovic, T., Curtis, J., Shumlas, S. L., Chatterjee, S., Intikhab, S., Chareev, D. A., Volkova, O. S., Vasiliev, A. N., Karapetrov, G. & Snyder, J. Tuning the activity/stability balance of anion doped CoSxSe2-x dichalcogenides. *J. Catal.* **366**, 50–60 (2018).

4. Stamenkovic, V. R., Fowler, B., Mun, B. S., Wang, G., Ross, P. N., Lucas, C. A. & Markovic, N. M. Improved Oxygen Reduction Activity on Pt3Ni(111) via Increased Surface Site Availability. *Science* **315**, 493–497 (2007).

5. Chatterjee, S., Griego, C., Hart, J. L., Li, Y., Taheri, M. L., Keith, J. & Snyder, J. D. Free Standing Nanoporous Palladium Alloys as CO Poisoning Tolerant Electrocatalysts for the Electrochemical Reduction of CO2 to Formate. *ACS Catal.* **9**, 5290–5301 (2019).

6. Koper, M. T. M. Thermodynamic theory of multi-electron transfer reactions : Implications for electrocatalysis. *J. Electroanal. Chem.* **660**, 254–260 (2011).

7. Garcı, J. M., Rossmeisl, J. & Koper, M. T. M. Physical and Chemical Nature of the Scaling Relations between Adsorption Energies of Atoms on Metal Surfaces. *Phys. Rev. Lett.* **108**, 116103 (2012).

8. Viswanathan, V. & Hansen, H. A. Unifying solution and surface electrochemistry: Limitations and opportunities in surface electrocatalysis. *Top. Catal.* **57**, 215–221 (2014).

9. Viswanathan, V., Hansen, H. A., Rossmeisl, J. & Nørskov, J. K. Unifying the 2e− and 4e− Reduction of Oxygen on Metal Surfaces. *J. Phys. Chem. Lett.* **3**, 2948–2951 (2012).

10. Tripkovic, V. Thermodynamic assessment of the oxygen reduction activity in aqueous solutions. *Phys. Chem. Chem. Phys.* **19**, 29381–29388 (2017).

11. Shao, M., Chang, Q., Dodelet, J. & Chenitz, R. Recent Advances in Electrocatalysts for Oxygen Reduction Reaction. *Chem. Rev.* **116**, 3594–3657 (2016).

12. Kim, D., Xie, C., Becknell, N., Yu, Y., Karamad, M., Chan, K., Crumlin, E. J., Nørskov, J. K. & Yang, P. Electrochemical Activation of CO2 through Atomic Ordering Transformations of AuCu Nanoparticles. *J. Am. Chem. Soc.* **139**, 8329–8336 (2017).

13. Liu, S., Tao, H., Liu, Q., Xu, Z., Liu, Q. & Luo, J. Rational Design of Silver Sul fi de Nanowires for E ffi cient CO 2 Electroreduction in Ionic Liquid. *ACS Catal.* **8**, 1469–1475 (2018).

14. Grote, J., Zeradjanin, A. R., Cherevko, S., Savan, A., Breitbach, B., Ludwig, A. & Mayrhofer, K. J. J. Screening of material libraries for electrochemical CO 2 reduction catalysts – Improving selectivity of Cu by mixing with Co. *J. Catal.* **343**, 248–256 (2016).

15. Li, M., Wang, J., Li, P., Chang, K., Li, C., Wang, T. & Jiang, B. electrodes for selective electrocatalytic reduction. *J. Mater. Chem. A* **4**, 4776–4782 (2016).

16. Yang, Y., Luo, M., Zhang, W., Sun, Y., Chen, X. & Guo, S. Metal Surface and Interface Energy Electrocatalysis : Fundamentals , Performance Engineering , and Opportunities. *Chem* **4**, 2054–2083 (2018).

17. Greaves, T. L. & Drummond, C. J. Protic ionic liquids: Properties and applications. *Chem. Rev.* **108**, 206–237 (2008).

18. Snyder, J., Livi, K. & Erlebacher, J. Oxygen reduction reaction performance of [MTBD][beti]-encapsulated nanoporous NiPt alloy nanoparticles. *Adv. Funct. Mater.* **23**, 5494–5501 (2013).

19. Snyder, J., Fujita, T., Chen, M. W. & Erlebacher, J. Oxygen reduction in nanoporous metal-ionic liquid composite electrocatalysts. *Nat. Mater.* **9**, 904–907 (2010).

20. Wang, T., Zhang, Y., Huang, B., Cai, B., Rao, R. R., Giordano, L., Sun, S. G. & Shao-Horn, Y. Enhancing oxygen reduction electrocatalysis by tuning interfacial hydrogen bonds. *Nat. Catal.* **4**, 753–762 (2021).

21. Izumi, R., Yao, Y., Tsuda, T., Torimoto, T. & Kuwabata, S. Pt-Nanoparticle-Supported Carbon Electrocatalysts Functionalized with a Protic Ionic Liquid and Organic Salt. *Adv. Mater. Interfaces* **5**, 1701123 (2018).

22. Li, Y., Hart, J., Profitt, L., Intikhab, S., Chatterjee, S., Taheri, M. & Snyder, J. Sequential Capacitive Deposition of Ionic Liquids for Conformal Thin Film Coatings on Oxygen Reduction Reaction Electrocatalysts. *ACS Catal.* **9**, 9311–9316 (2019).

23. Benn, E., Uvegi, H. & Erlebacher, J. Characterization of Nanoporous Metal-Ionic Liquid Composites for the Electrochemical Oxygen Reduction Reaction. *J. Electrochem. Soc.* **162**, H759–H766 (2015).

24. George, M., Zhang, G. R., Schmitt, N., Brunnengräber, K., Sandbeck, D. J. S., Mayrhofer, K. J. J., Cherevko, S. & Etzold, B. J. M. Effect of Ionic Liquid Modification on the ORR Performance and Degradation Mechanism of Trimetallic PtNiMo/C Catalysts. *ACS Catal.* **9**, 8682–8692 (2019).

25. Huang, K., Song, T., Morales-Collazo, O., Jia, H. & Brennecke, J. F. Enhancing Pt/C Catalysts for the Oxygen Reduction Reaction with Protic Ionic Liquids: The Effect of Anion Structure. *J. Electrochem. Soc.* **164**, F1448–F1459 (2017).

26. Zhang, G., Munoz, M. & Etzold, B. J. M. Boosting Performance of Low Temperature Fuel Cell Catalysts by Subtle Ionic Liquid Modification. *ACS Appl. Mater. Interfaces* **7**, 3562–3570 (2015).

27. Zhang, G. R., Munoz, M. & Etzold, B. J. M. Accelerating oxygen-reduction catalysts through preventing poisoning with non-reactive species by using hydrophobic ionic liquids. *Angew. Chemie - Int. Ed.* **55**, 2257–2261 (2016).

28. Wang, M., Zhang, H., Thirunavukkarasu, G., Salam, I., Varcoe, J. R., Mardle, P., Li, X., Mu, S. & Du, S. Ionic Liquid-Modified Microporous ZnCoNC-Based Electrocatalysts for Polymer Electrolyte Fuel Cells. *ACS Energy Lett.* **4**, 2104–2110 (2019).

29. Qiao, M., Ferrero, G. A., Fernández Velasco, L., Vern Hor, W., Yang, Y., Luo, H., Lodewyckx, P., Fuertes, A. B., Sevilla, M. & Titirici, M. M. Boosting the Oxygen Reduction Electrocatalytic Performance of Nonprecious Metal Nanocarbons via Triple Boundary Engineering Using Protic Ionic Liquids. *ACS Appl. Mater. Interfaces* **11**, 11298–11305 (2019).

30. Subbaraman, R., Strmcnik, D., Stamenkovic, V. & Markovic, N. M. Three Phase Interfaces at Electrified Metal - Solid Electrolyte Systems 1 . Study of the Pt (hkl) - Nafion Interface. *J. Phys. Chem. C* **114**, 8414–8422 (2010).

31. Subramanian, N. P., Greszler, T. A., Zhang, J., Gu, W. & Makharia, R. Pt-Oxide Coverage-Dependent Oxygen Reduction Reaction (ORR) Kinetics. *J. Electrochem. Soc.* **159**, B531–B540 (2012).

32. Stamenković, V., Schmidt, T. J., Ross, P. N. & Marković, N. M. Surface composition effects in electrocatalysis: Kinetics of oxygen reduction on well-defined Pt3Ni and Pt3Co alloy surfaces. *J. Phys. Chem. B* **106**, 11970–11979 (2002).

33. Marković, N. M., Gasteiger, H. A., Grgur, B. N. & Ross, P. N. Oxygen reduction reaction on Pt(111): effects of bromide. *J. Electroanal. Chem.* **467**, 157–163 (1999).

34. Wakisaka, M., Udagawa, Y., Suzuki, H., Uchida, H. & Watanabe, M. Structural effects on the surface oxidation processes at Pt single-crystal electrodes studied by X-ray photoelectron spectroscopy. *Energy Environ. Sci.* **4**, 1662–1666 (2011).

35. Ueno, T., Tanaka, H., Sugawara, S., Shinohara, K., Ohma, A., Hoshi, N. & Nakamura, M. Infrared spectroscopy of adsorbed OH on n(111)–(100) and n(111)–(111) series of Pt electrode. *J. Electroanal. Chem.* **800**, 162–166 (2017).

36. Tanaka, H., Sugawara, S., Shinohara, K., Ueno, T., Suzuki, S., Hoshi, N. & Nakamura, M. Infrared Reflection Absorption Spectroscopy of OH Adsorption on the Low Index Planes of Pt. *Electrocatalysis* **6**, 295–299 (2015).

37. Markovic, N., Gasteiger, H., Ross, P. N., Berkeley, L. & Division, M. S. Kinetics of Oxygen Reduction on Pt (hkl) Electrodes : Implications for the Crystallite Size Effect with Supported Pt Electrocatalysts. *J. Electrochern. Soc* **144**, 1591–1597 (1997).

38. Stamenkovic, V., Mun, B. S., Mayrhofer, K. J. J., Ross, P. N., Markovic, N. M., Rossmeisl, J., Greeley, J. & Nørskov, J. K. Changing the activity of electrocatalysts for oxygen reduction by tuning the surface electronic structure. *Angew. Chemie - Int. Ed.* **45**, 2897–2901 (2006).

39. Kuzume, A., Herrero, E. & Feliu, J. M. Oxygen reduction on stepped platinum surfaces in acidic media. *J. Electroanal. Chem.* **599**, 333–343 (2007).

40. Markovic, N. M., Gasteiger, H. A. & Ross, P. N. Oxygen reduction on platinum low-index single-crystal surfaces in sulfuric acid solution. Rotating ring - Pt(hkl) disk studies. *J. Phys. Chem.* **99**, 3411–3415 (1995).

41. Viswanathan, V., Hansen, H. A., Rossmeisl, J. & Nørskov, J. K. Universality in oxygen reduction electrocatalysis on metal surfaces. *ACS Catal.* **2**, 1654–1660 (2012).

42. Zhu, T., Sun, S. G., Van Santen, R. A. & Hensen, E. J. M. Reconstruction of clean and oxygen-covered Pt(110) surfaces. *J. Phys. Chem. C* **117**, 11251–11257 (2013).

43. García, G. & Koper, M. T. M. Carbon monoxide oxidation on Pt single crystal electrodes: Understanding the catalysis for low temperature fuel cells. *ChemPhysChem* **12**, 2064–2072 (2011).

44. Gómez-Marín, A. M., Rizo, R. & Feliu, J. M. Oxygen reduction reaction at Pt single crystals: A critical overview. *Catal. Sci. Technol.* **4**, 1685–1698 (2014).

45. Markovic, N. M., Adzic, R. R., Cahan, B. D. & Yeager, E. B. Structural effects in electrocatalysis: oxygen reduction on platinum low index single-crystal surfaces in perchloric acid solutions. *J. Electroanal. Chem.* **377**, 249–259 (1994).

46. Casalongue, H. S., Kaya, S., Viswanathan, V., Miller, D. J., Friebel, D., Hansen, H. A., Nørskov, J. K., Nilsson, A. & Ogasawara, H. Direct observation of the oxygenated species during oxygen reduction on a platinum fuel cell cathode. *Nat. Commun.* **4**, 1–6 (2013).

47. Schiros, T. & Andersson, K. J. Cooperativity in Surface Bonding and Hydrogen Bonding of Water and Hydroxyl at Metal Surfaces. *J. Phys. Chem. C* **114**, 10240–10248 (2010).

48. Andersson, K., Gyllenpalm, J., Karlberg, G. S. & Odelius, M. Structure and Bonding of the Water - Hydroxyl Mixed Phase on Pt (111). *J. Phys. Chem. C* **111**, 15003–15012 (2007).

49. Bondarenko, A. S., Stephens, I. E. L., Hansen, H. A., Francisco, J. P., Tripkovic, V., Johansson, T. P., Rossmeisl, J., Nørskov, J. K. & Chorkendorff, I. The Pt (111) / Electrolyte Interface under Oxygen Reduction Reaction Conditions : An Electrochemical Impedance Spectroscopy Study. *Langmuir* **27**, 2058–2066 (2011).

50. Ogasawara, H., Kaya, S. & Nilsson, A. Operando X-Ray Photoelectron Spectroscopy Studies of Aqueous Electrocatalytic Systems. *Top. Catal.* **59**, 439–447 (2016).

51. Kumeda, T., Tajiri, H., Sakata, O., Hoshi, N. & Nakamura, M. Effect of hydrophobic cations on the oxygen reduction reaction on single-crystal platunum electrode. *Nat. Commun.* **9**, 4378 (2018).

52. Ledezma-yanez, I., Wallace, W. D. Z., Sebastián-pascual, P., Climent, V., Feliu, J. M. & Koper, M. T. M. Interfacial water reorganization as a pH-dependent descriptor of the hydrogen evolution rate on platinum electrodes. *Nat. Energy* **2**, 17031 (2017).

53. Pecina, O. & Schmickler, W. A model for electrochemical proton-transfer reactions. *Chem. Phys.* **228**, 265–277 (1998).

54. Gómez, R., Orts, J. M., Álvarez-Ruiz, B. & Feliu, J. M. Effect of temperature on hydrogen adsorption on Pt(111), Pt(110), and Pt(100) electrodes in 0.1 M HClO4. *J. Phys. Chem. B* **108**, 228–238 (2004).

55. Kim, Y., Shin, S. & Kang, H. Zundel-like and Eigen-like Hydrated Protons on a Platinum Surface. *Angew. Chemie Int. Ed.* **54**, 7626–7630 (2015).

56. Chu, Y. S., Lister, T. E., Cullen, W. G., You, H. & Nagy, Z. Commensurate Water Monolayer at the RuO2 (110)/ˆ¯Water Interface. *Phys. Rev. Lett.* **86**, 3364–3368 (2001).

57. Bjo, O., Hansen, M. H., Hodgson, A., Liu, L., Limmer, D. T., Michaelides, A., Pedevilla, P., Rossmeisl, J., Shen, H., Tocci, G., Tyrode, E., Walz, M., Werner, J. & Bluhm, H. Water at Interfaces. *Chem. Rev.* **116**, 7698–7726 (2016).

58. Badan, C., Heyrich, Y., Koper, M. T. M. & Juurlink, L. B. F. Surface Structure Dependence in Desorption and Crystallization of Thin Interfacial Water Films on Platinum. *J. Phys. Chem. Lett.* **7**, 1682–1685 (2016).

59. Schwarz, K., Xu, B., Yan, Y. & Sundararaman, R. Partial oxidation of step-bound water leads to anomalous pH effects on metal electrode step-edges. *Phys. Chem. Chem. Phys.* **18**, 16216–16223 (2016).

60. Yeh, K., Wasileski, A. & Janik, M. J. Electronic structure models of oxygen adsorption at the solvated , electrified Pt (111) interface. *Phys. Chem. Chem. Phys.* **11**, 10108–10117 (2009).

61. Zeng, Z. & Greeley, J. Characterization of oxygenated species at water/Pt(111) interfaces from DFT energetics and XPS simulations Zhenhua. *Nano Energy* **29**, 369–377 (2016).

62. Niet, M. J. T. C. Van Der, Garcia-araez, N., Hernández, J., Feliu, J. M. & Koper, M. T. M. Water dissociation on well-defined platinum surfaces : The electrochemical perspective. *Catal. Today* **202**, 105–113 (2013).

63. Luo, H., Baker, G. A., Lee, J. S., Pagni, R. M. & Dai, S. Ultrastable Superbase-Derived Protic Ionic Liquids. *J. Phys. Chem. B* **113**, 4181–4183 (2009).

64. Malkani, A. S., Dunwell, M. & Xu, B. Operando Spectroscopic Investigations of Copper and Oxide-Derived Copper Catalysts for Electrochemical CO Reduction. *ACS Catal.* **9**, 474–478 (2018).

65. Dunwell, M., Yan, Y. & Xu, B. A surface-enhanced infrared absorption spectroscopic study of pH dependent water adsorption on Au. *Surf. Sci.* **650**, 51–56 (2016).

66. Ataka, K. & Osawa, M. In Situ Infrared Study of Water - Sulfate Coadsorption on Gold(111) in Sulfuric Acid Solutions. *Langmuir* **14**, 951–959 (1998).

67. Ataka, K., Yotsuyanagi, T. & Osawa, M. Potential-Dependent Reorientation of Water Molecules at an Electrode / Electrolyte Interface Studied by Surface-Enhanced Infrared Absorption Spectroscopy. *J. Phys. Chem.* **100**, 10664–10672 (1996).

68. Iwasita, T. & Xia, X. Adsorption of water at Pt(111) electrode in HClO4 solutions. the potential of zero charge. *J. Electroanal. Chem.* **411**, 95–102 (1996).

69. Shingaya, Y. & Ito, M. Simulation of the electric double layers on Pt(111). *Surf. Sci.* **386**, 34–47 (1997).

70. Zheng, W. & Tadjeddine, A. Adsorption processes and structure of water molecules on Pt(110) electrodes in perchloric solutions. *J. Chem. Phys.* **119**, 13096–13099 (2003).

71. Futamata, M., Luo, L. & Nishihara, C. ATR-SEIR study of anions and water adsorbed on platinum electrode. *Surf. Sci.* **590**, 196–211 (2005).

72. Osawa, M., Tsushima, M., Mogami, H., Samjeské, G. & Yamakata, A. Structure of water at the electrified platinum-water interface: A study by surface-enhanced infrared absorption spectroscopy. *J. Phys. Chem. C* **112**, 4248–4256 (2008).

73. Freire, M. G., Neves, C. M. S. S., Carvalho, P. J., Gardas, R. L., Fernandes, A. M., Marrucho, I. M., Santos, L. M. N. B. F. & Coutinho, J. A. P. Mutual solubilities of water and hydrophobic ionic liquids. *J. Phys. Chem. B* **111**, 13082–13089 (2007).

74. Hayes, R., Imberti, S., Warr, G. G. & Atkin, R. How Water Dissolves in Protic Ionic Liquids. *Angew. Chemie* **124**, 7586–7589 (2012).

75. Nakamura, M., Nakajima, Y., Hoshi, N., Tajiri, H. & Sakata, O. Effect of Non-Specifically Adsorbed Ions on the Surface Oxidation of Pt (111). *ChemPhysChem* **14**, 2426–2431 (2013).

76. Weber, D. J., Janssen, M. & Oezaslan, M. Effect of Monovalent Cations on the HOR / HER Activity for Pt in Alkaline Environment. *J. Electrochem. Soc* **166**, F66–F73 (2019).

77. Chen, X., McCrum, I. T., Schwarz, K. A., Janik, M. J. & Koper, M. T. M. Co-adsorption of Cations as the Cause of the Apparent pH Dependence of Hydrogen Adsorption on a Stepped Platinum Single-Crystal Electrode. *Angew. Chemie - Int. Ed.* **56**, 15025–15029 (2017).

78. McCrum, I. T. & Janik, M. J. pH and Alkali Cation Effects on the Pt Cyclic Voltammogram Explained Using Density Functional Theory. *J. Phys. Chem. C* **120**, 457–471 (2016).

79. Katsounaros, I., Schneider, W. B., Meier, J. C., Benedikt, U., Biedermann, P. U., Auer, A. & Mayrhofer, K. J. J. Hydrogen peroxide electrochemistry on platinum : towards

understanding the oxygen reduction reaction mechanism w. *Phys. Chem. Chem. Phys.* **14**, 7384–7391 (2012).

80. Panchenko, A., Koper, M. T. M., Shubina, T. E. & Mitchell, S. J. Ab Initio Calculations of Intermediates of Oxygen Reduction on Low-Index Platinum Surfaces. *J. Electrochem. Soc* **151**, A2016–A2027 (2004).

81. Li, X., Heryadi, D. & Gewirth, A. A. Electroreduction Activity of Hydrogen Peroxide on Pt and Au Electrodes. *Langmuir* **21**, 9251–9259 (2005).

82. Gawas, R., Snyder, J. & Tang, M. Modifying Interface Solvation and Oxygen Reduction Electrocatalysis with Hydrophobic Species. *J. Phys. Chem. C* **126**, 14509–14517 (2022).

83. Zhang, G. R., Wolker, T., Sandbeck, D. J. S., Munoz, M., Mayrhofer, K. J. J., Cherevko, S. & Etzold, B. J. M. Tuning the Electrocatalytic Performance of Ionic Liquid Modified Pt Catalysts for the Oxygen Reduction Reaction via Cationic Chain Engineering. *ACS Catal.* **8**, 8244–8254 (2018).

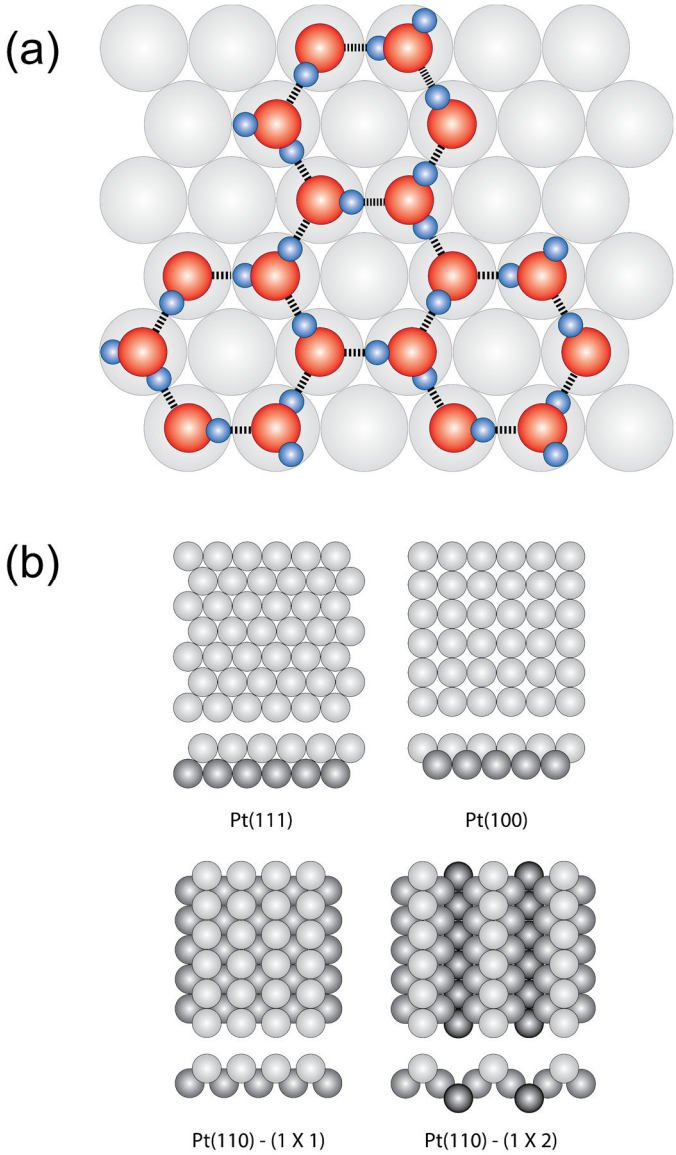

Figure 1: (a) Schematic of ordered ice-like hydrogen bonded water structure with OH_{ad} on a (111) close packed plane. (b) Schematic representation of top view and side view of the atomic geometry of Pt(111), Pt(100), Pt(110) – (1X1), and Pt(110) – (1X2) surfaces.

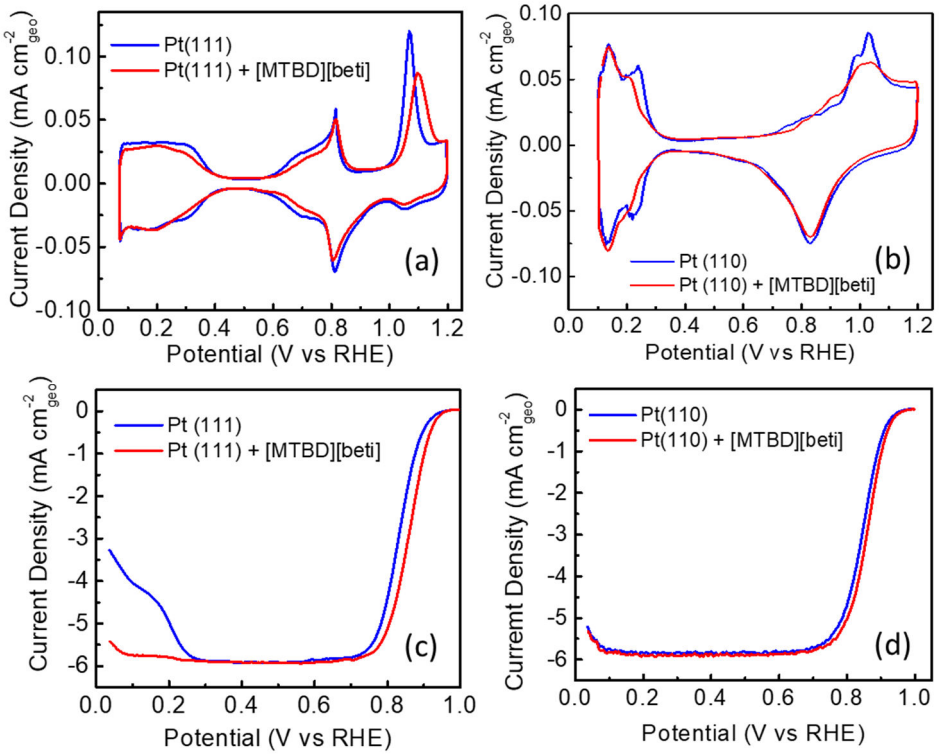

Figure 2: (a) CVs of Pt (111) (blue) and Pt (111) + [MTBD][beti] (red) in Ar saturated 0.1 M $HClO_4$ with scan rate of 50 mV s^{-1}; (b) CVs of Pt (110) (blue) and Pt (110) + [MTBD][beti] (red) in Ar saturated 0.1 M $HClO_4$ with scan rate of 50 mV s^{-1}; (c) ORR polarization curves of Pt (111) (blue) and Pt (111) + [MTBD][beti] (red) in O_2 saturated 0.1 M $HClO_4$ at 1600 rpm with scan rate of 20 mV s^{-1}; (d) ORR polarization curves of Pt (110) (blue) and Pt (110) + [MTBD][beti] (red) in O_2 saturated 0.1 M $HClO_4$ at 1600 rpm with scan rate of 20 mV s^{-1}.

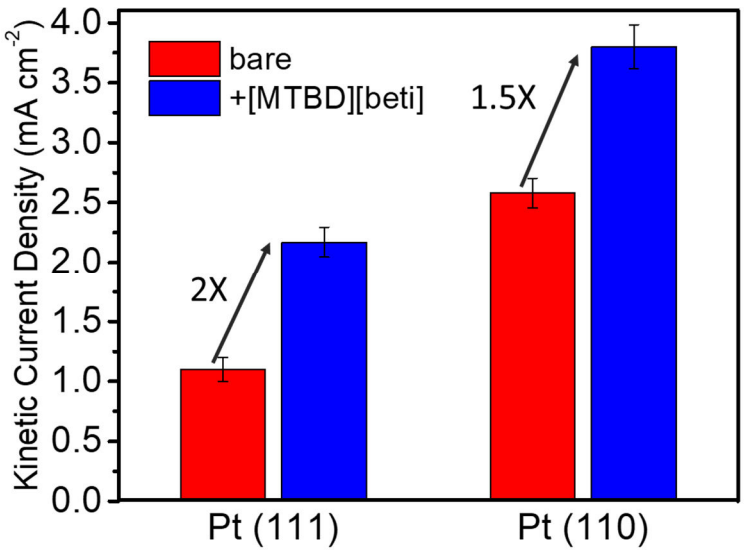

Figure 3: Improvement of ORR kinetic current density at 0.9 V vs. RHE for Pt (111) and Pt (110) with IL [MTBD][beti] coated.

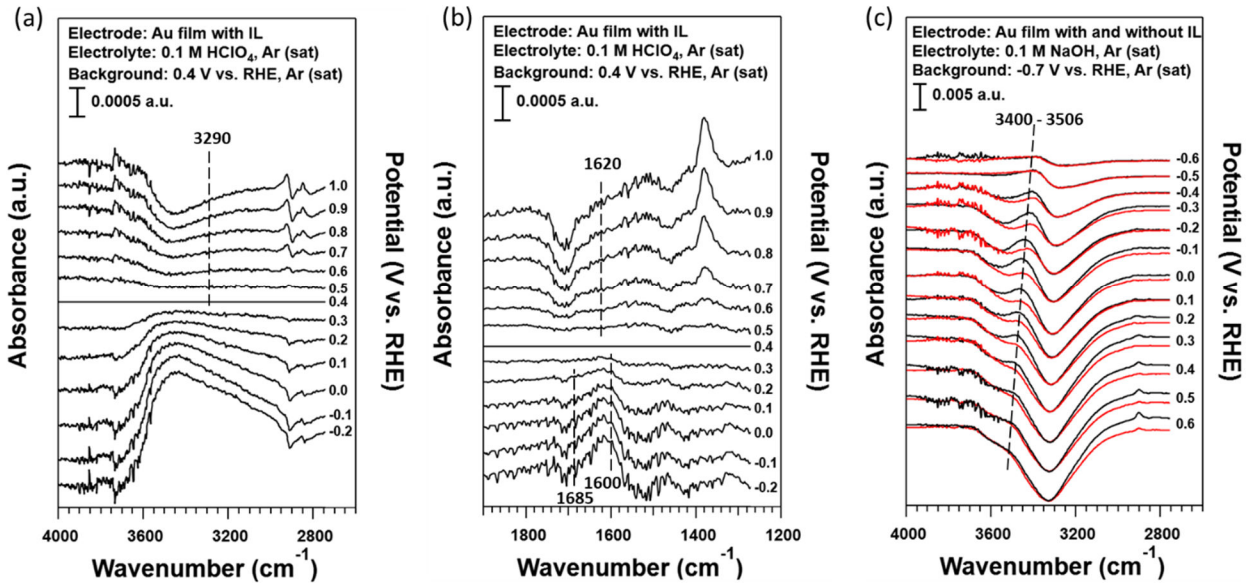

Figure 4: ATR-SEIRAS spectra of the potential dependent behavior of (a) and (b) interfacial water in Ar saturated 0.1 M $HClO_4$ on Au + [MTBD][beti] film electrode and (c) adsorbed OH in Ar saturated 0.1 M NaOH on Au (black) and Au + [MTBD][beti] (red) film electrodes.

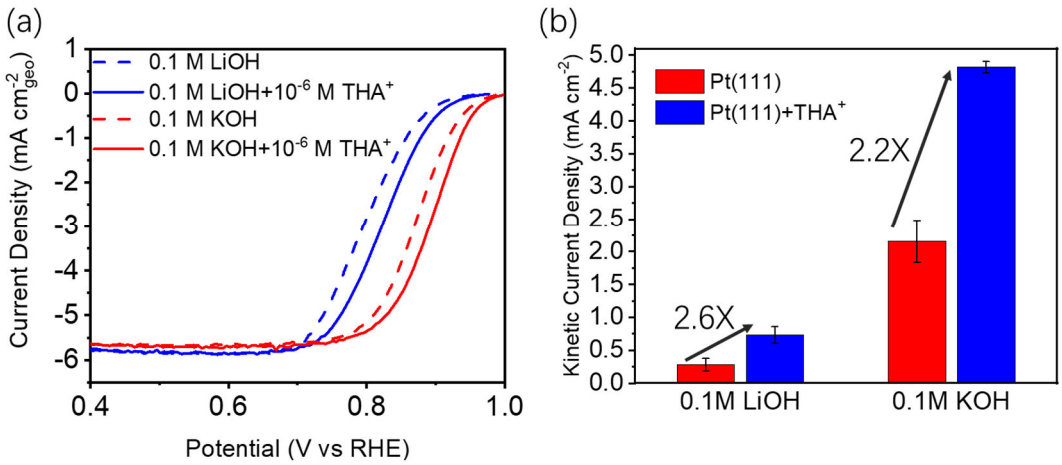

Figure 5. (a) the ORR polarization curves of Pt (111) in 0.1 M LiOH (dash blue) and 0.1 M KOH (dash red) comparing with Pt (111) in 0.1 M LiOH containing 10^{-6} M THA^+ (solid blue) and Pt (111) in 0.1 M KOH containing 10^{-6} M THA^+ (solid red). Linear sweep voltammograms were obtained in the O_2 saturated electrolyte at 1600 rpm with scan rate of 20 mV s^{-1}. (b) Improvement of ORR kinetic current density at 0.9 V vs. RHE for Pt (111) between bare and THA^+ for 0.1 M LiOH and 0.1M KOH.

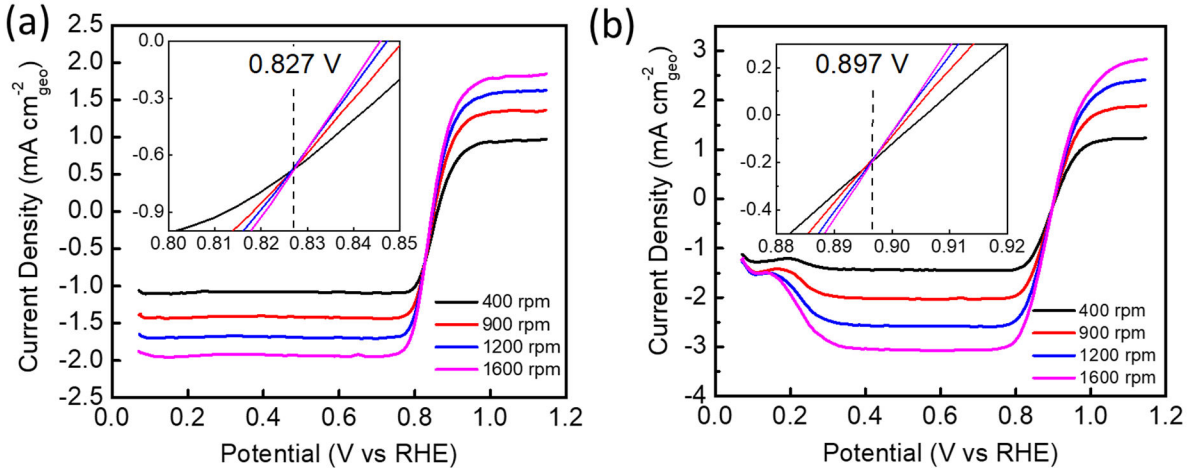

Figure 6: Anodic scan of cyclic voltammograms for (a) bare Pt (110) and (b) Pt (110) + [MTBD][beti] in Ar saturated 0.1 M $HClO_4$ + 2 mM H_2O_2 at indicated rotation rate with scan rate of 20 mV s^{-1}.

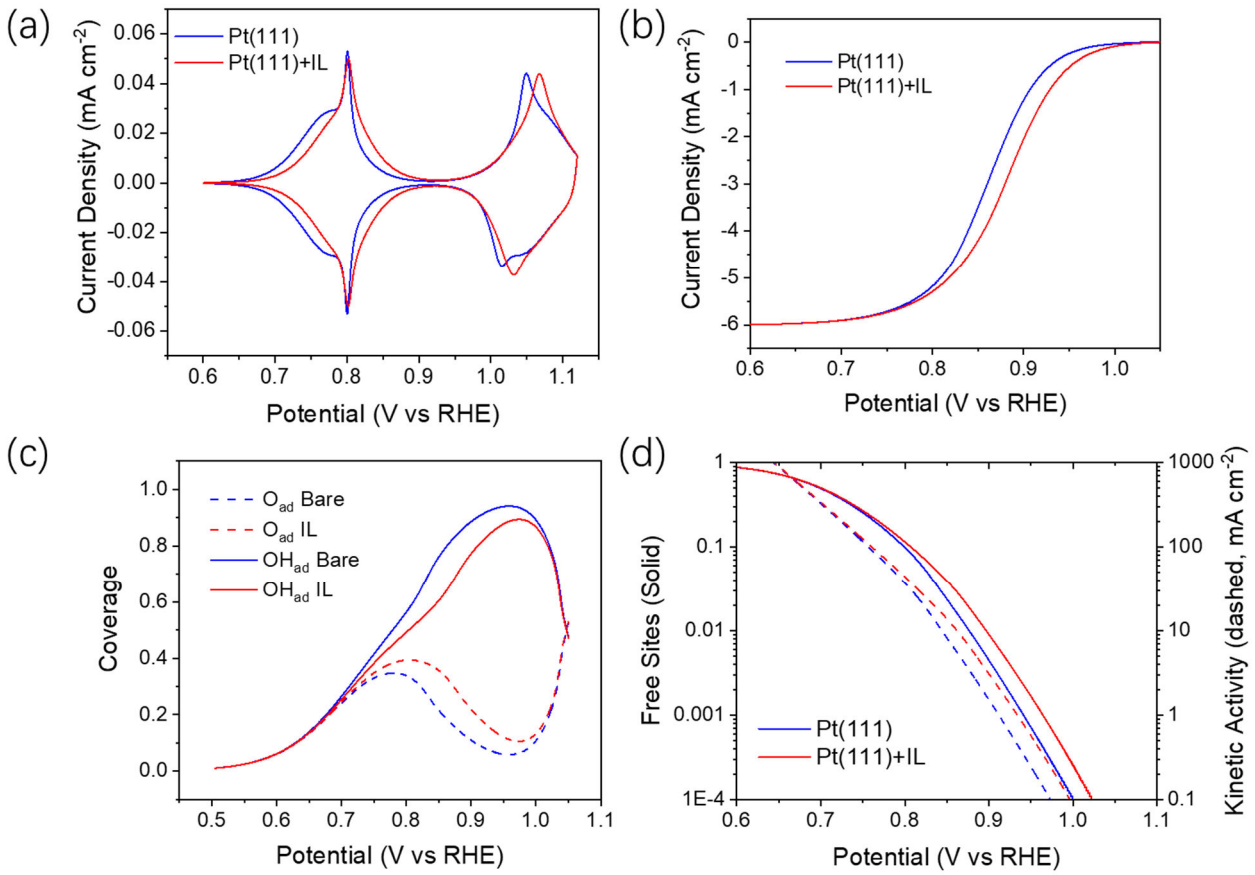

Figure 7: Simulated (a) CVs, (b) ORR polarization curves, (c) potential dependent equilibrium coverages of adsorbed oxygenated species, and (d) coverage of free-sites and kinetic activity plots as a function of potential for Pt(111) (blue) and Pt(111) + IL (red) during ORR .

TOC Graphic

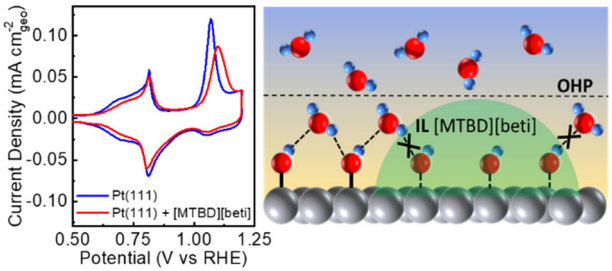
Current Density (mA cm$^{-2}_{geo}$)
0.10
0.05
0.00
-0.05
-0.10
Pt(111)
Pt(111) + [MTBD][beti]
0.50
0.75
1.00
1.25
Potential (V vs RHE)
OHP
IL [MTBD][beti]